

Hole-subband mixing in quantum wells: A magneto-optic study

F. Ancilotto and A. Fasolino

International School for Advanced Studies, Strada Costiera 11, I-34100 Trieste, Italy

J. C. Maan

Max-Planck-Institut für Festkörperforschung, Hochfeld Magnetlabor, 166X F38042 Grenoble Cedex, France

(Received 5 June 1987; revised manuscript received 29 February 1988)

The effect of mixing of the hole subbands on the magneto-optical interband transitions in quantum wells is investigated in a six-band envelope-function approach. Our results compare favorably with magneto-optical experiments on GaAs quantum wells and help considerably in their understanding. In particular, the explicit evaluation of the transition strengths is necessary in order to explain the experimental findings: The relaxation of the usual selection rules for optical transitions due to the strong mixing between the hole subbands has a remarkable effect on the observed absorption spectra and is well accounted for by our calculation. Excitonic effects due to the electron-hole Coulomb interaction are included in a simplified manner. A higher band-edge electron mass is needed in order to fit the experimental data; we believe that this is an indication that nonparabolicity effects are stronger than usually assumed.

I. INTRODUCTION

The recent improvement in epitaxial growth techniques has made it possible to realize high-quality semiconductor heterostructures. The dispersion of the hole subbands in these structures is rather interesting because the degeneracy of the bulk valence bands and the effect of the confinement in the one-dimensional superlattice (SL) potential combine to produce strong nonparabolicities.^{1,2} At the same time the confinement energy of the electrons in the conduction band enhances the effect of band nonparabolicity with respect to the bulk.

Many of the most revealing experiments on semiconductor heterostructures are performed in an external magnetic field: in a two dimensional (2D) system of electrons or holes in an isolated quantum well (QW) or in the binding potential at the interface of a doped heterojunction, a perpendicular magnetic field quantizes both available degrees of freedom, producing an entirely discrete spectrum and thus leading to an enrichment of optical structures.^{3,4}

Magneto-optical experiments on these systems have revealed in the observed spectra complex features that cannot be accounted for by simple models of quantum confinement. More detailed band-structure calculations are necessary in order to explain the observed spectra: However, the strong nonlinear behavior of the Landau levels and the relaxation of the usual selection rules for optical transitions resulting from the coupling between heavy-hole (HH) and light-hole (LH) subbands, have precluded up to now a convincing comparison between theory and experiments.⁵ In addition, the interpretation of magneto-optical data in terms of single-effective masses to describe the HH and LH dispersions has masked somewhat the effect of nonparabolicity in the conduction subbands.

The purpose of the present paper is to show which

effects are brought about by the mixing of the valence subbands in quantum wells on interband magneto-optical transitions. The system investigated is a GaAs/Al_xGa_{1-x}As QW in an external magnetic field applied along the (001) growth axis and the results of the calculations are compared with the experiments.

The quantitative details of the calculation depend critically on the sample parameters, implying the possibility of their precise determination through the comparison between the theory and magneto-optical experiments. In particular, the combined check against the energy positions and the intensities of the transitions allows one to assign unambiguously every experimental transition line to a calculated one and also to estimate the HH₁ exciton binding energy.

The paper is organized as follows: In Sec. II the method of calculation of Landau levels in a QW is briefly outlined; in Sec. III we discuss the resulting nonlinear electron and hole Landau levels; in Sec. IV we evaluate explicitly the matrix elements for direct optical transitions between valence-to-conduction Landau levels and make simple considerations about the symmetry properties of the SL wavefunction; Sec. V is devoted to the comparison between theory and magneto-optical experiments; by including the exciton effect in a simple model,^{3,6} we are able to reproduce many details of the observed spectra; in Sec. VI some concluding remarks are given.

II. THEORY

The method of calculation, based on a six-band envelope-function approach, is described in detail elsewhere.^{2,7,8}

Assuming a full $\mathbf{k}\cdot\mathbf{p}$ coupling between a twofold s -like conduction band and the upper ($J = \frac{3}{2}$) fourfold edge of a spin-orbit-split p -like valence band at $\mathbf{k}=\mathbf{0}$, the bulk band structure of a direct-gap semiconductor in the presence of

a magnetic field applied in the $\langle 001 \rangle$ direction (hereafter denoted by z) is described in terms of a 6×6 effective matrix Hamiltonian H (additional terms that come from the lack of inversion symmetry in zinc-blende semiconduc-

tors⁹ are neglected, as usual):

$$H = H_{\text{ax}} + H_{\text{cub}}, \quad (1)$$

where (atomic units are used throughout the paper)

$$H_{\text{ax}} = \begin{pmatrix} H_{11} & iP\sqrt{eB/c}a^\dagger & iP\sqrt{eB/3c}a & 0 & -iP\sqrt{2/3}k_z & 0 \\ & H_{22} & \bar{\gamma}\sqrt{3}(eB/c)a^2 & 0 & \gamma_3\sqrt{6eB/c}k_z a & 0 \\ & & H_{33} & iP\sqrt{2/3}k_z & 0 & -\gamma_3\sqrt{6eB/c}k_z a \\ & & & H_{44} & iP\sqrt{eB/3c}a^\dagger & -iP\sqrt{eB/c}a \\ & & & & H_{55} & \bar{\gamma}\sqrt{3}(eB/c)a^2 \\ & & & & & H_{66} \end{pmatrix}, \quad (1a)$$

$$H_{11} = H_{44} = E_c + (eB/m_{\text{s.o.}}c)(a^\dagger a + 1) + k_z^2/2m_{\text{s.o.}},$$

$$H_{22} = E_v - (\gamma_1/2 - \gamma_2)k_z^2 - (eB/c)[(\gamma_1 + \gamma_2)(a^\dagger a + \frac{1}{2}) + 3\kappa/2],$$

$$H_{33} = E_v - (\gamma_1/2 + \gamma_2)k_z^2 - (eB/c)[(\gamma_1 - \gamma_2)(a^\dagger a + \frac{1}{2}) - \kappa/2],$$

$$H_{55} = E_v - (\gamma_1/2 + \gamma_2)k_z^2 - (eB/c)[(\gamma_1 - \gamma_2)(a^\dagger a + \frac{1}{2}) + \kappa/2],$$

$$H_{66} = E_v - (\gamma_1/2 - \gamma_2)k_z^2 - (eB/c)[(\gamma_1 + \gamma_2)(a^\dagger a + \frac{1}{2}) - 3\kappa/2],$$

and the lower half of the matrix is obtained by Hermitian conjugation. In (1a) $\bar{\gamma} = (\gamma_2 + \gamma_3)/2$, E_c and E_v are the conduction and valence band-edge energies, B is the magnetic field strength, a and a^\dagger are harmonic oscillator raising and lowering operators; five band parameters, $P \equiv -i \langle s | p_x | x \rangle$, γ_1 , γ_2 , γ_3 , and κ appear in this matrix, describing electron and hole effective masses and g factors. The effective mass $m_{\text{s.o.}}^{-1} = 1 + 2P^2/3(E_g + \Delta)$ appearing in the electron terms H_{11} and H_{44} takes into account indirectly the coupling to the split-off ($J = \frac{1}{2}$) band,¹⁰ E_g and Δ being, respectively, the energy gap and the spin-orbit splitting at $\mathbf{k} = 0$.

The term H_{cub} has the form

$$H_{\text{cub}} = \begin{pmatrix} H_a & 0 \\ 0 & H_a \end{pmatrix}, \quad (1b)$$

where

$$H_a = \frac{\sqrt{3}eB}{2c}(\gamma_2 - \gamma_3) \begin{pmatrix} 0 & 0 & 0 \\ 0 & 0 & (a^\dagger)^2 \\ 0 & a^2 & 0 \end{pmatrix}.$$

Inclusion of this anisotropic term uncrosses some of the Landau levels, namely those differing in the Landau index n by ± 4 , but the absolute shifts are always less than 10%.^{11,12} We will then assume $H_{\text{cub}} = 0$.

The H_{ax} term in (1), which neglects the anisotropy in the (k_x, k_y) plane, can be solved exactly. In this case the solution of the effective-mass (EM) equation in each of the A and B materials constituting the SL takes the form^{2,13}

$$F_n = (c_1(z)\phi_n, c_2(z)\phi_{n-1}, c_3(z)\phi_{n+1}, c_4(z)\phi_{n+1}, c_5(z)\phi_n, c_6(z)\phi_{n+2}), \quad (2)$$

where $\phi_n(x, y)$ are harmonic oscillator wave functions with $n = -2, -1, 0, \dots$ and the $c_j(z)$ coefficients are automatically vanishing for the components with negative oscillator index.

With the replacement $k_z \equiv k_{sz} - i \partial/\partial z$ in H_{ax} (k_{sz} being the quasimomentum in the SL Brillouin zone), the EM equations for the components F_n^i of (2) become a system of differential equations for the envelope functions $c_j(z)$. Suitable current-conserving boundary conditions

must be imposed at the interfaces.⁷

The total zeroth-order wave function is

$$\Psi_n = e^{ik_{sz}z} \sum_{j=1}^6 F_n^j u_j, \quad (3a)$$

where u_j is the periodic part of the j th host Bloch function; our basis is⁷

$$\begin{aligned}
u_1 &= |s \uparrow \rangle, \\
u_2 &= \left| \frac{3}{2}; \frac{3}{2} \right\rangle = | -\sqrt{1/2}(x + iy) \uparrow \rangle, \\
u_3 &= \left| \frac{3}{2}, -\frac{1}{2} \right\rangle = | -\sqrt{1/6}(x - iy) \uparrow - \sqrt{2/3}z \downarrow \rangle, \\
u_4 &= |s \downarrow \rangle, \\
u_5 &= \left| \frac{3}{2}; \frac{1}{2} \right\rangle = | -\sqrt{2/3}z \uparrow + \sqrt{1/6}(x + iy) \downarrow \rangle, \\
u_6 &= \left| \frac{3}{2}; -\frac{3}{2} \right\rangle = | -\sqrt{1/2}(x - iy) \downarrow \rangle
\end{aligned} \tag{3b}$$

(these functions are assumed to be identical in A and B layers, in the spirit of the envelope function approach). For SL's with very thick barriers (QW limit), the dependence on k_{sz} of (3) is very small and can be neglected.

III. LANDAU LEVELS IN QUANTUM WELLS

The calculated hole and electron Landau levels (LL) for the case of a 78-Å QW between $\text{Al}_{0.3}\text{Ga}_{0.7}\text{As}$ barriers are shown in Figs. 1(a) and 1(b) (the zero of energy is taken at the top of the GaAs valence band). They are obtained using a 60%-40% rule for the band offset; the material parameters used are listed in Table I.

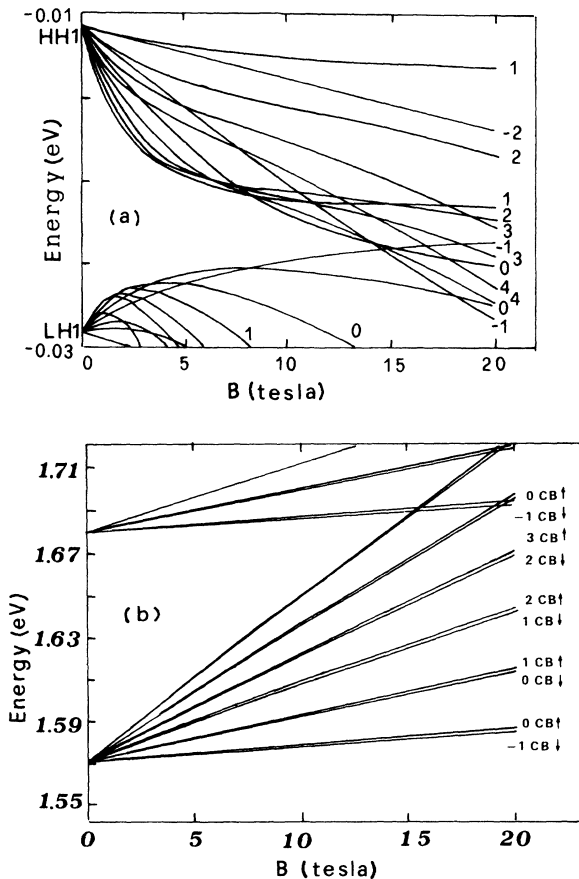


FIG. 1. (a) Calculated Landau levels for the first two hole subbands in a 78-Å GaAs QW between 160-Å $\text{Al}_{0.3}\text{Ga}_{0.7}\text{As}$ barriers. The numbers are the Landau level indices n . (b) Calculated Landau levels for the first two electron subbands. The two spin-split states are also indicated for each level.

TABLE I. Material parameters used in the calculations.

	Band parameters	
	GaAs	AlAs ^a
P (a.u.)	8.78 ^b	8.78
γ_1 (a.u.)	2.41	1.29
γ_2 (a.u.)	-0.12	-0.40
γ_3 (a.u.)	0.68	0.21
κ (a.u.)	-1.02	-0.96
E_g (eV)	1.53 ^c	3.13 ^d
Δ (eV)	0.34	0.27

^aLinear interpolation is used for $\text{Al}_x\text{Ga}_{1-x}\text{As}$.

^bCorresponding to the value $m^* = 0.074$ for the electron mass (see text).

^cThe energy gap of GaAs at 0 K is 1.52 eV: The 10 meV difference is due to the presence of a slight amount ($\leq 1\%$) of Al in the GaAs well of the sample analyzed.

^dThe energy gap for $\text{Al}_x\text{Ga}_{1-x}\text{As}$ is (Ref. 41) $E_g(x) = E_g^{\text{GaAs}} + 1.155x + 0.37x^2$.

A. Holes

The most remarkable feature of the calculated hole LL displayed in Fig. 1(a) is their strong nonlinear dependence on the magnetic field.² At $B \neq 0$, LL's originating from the first HH subband interact with those from the next subbands, giving rise to anticrossing behavior. In particular, the initial electronlike dispersion of LL's emerging from the LH1 subband is mainly due to the interaction between LH1 and the HH2 subbands (see Appendix A). It is evident that this Landau-level structure can no longer be described in terms of one effective mass per subband.

B. Electrons

The Landau levels for the conduction subbands shown in Fig. 1(b) are much more regular with respect to the ones derived for holes, displaying a simple "Landau ladder" form [note that a scale of energy different from Fig. 1(a) has been used]: At high fields slight deviations from a linear behavior occur, especially for large n ; in particular, the separation between successive levels, at a fixed value of B , decreases with increasing n .

These effects, as it is well known, must be ascribed to nonparabolicity in the conduction band due to the coupling with valence-band states. In fact, the energy of the electron levels—measured from the conduction subband edges at $B=0$ —can be approximated as well by the following expression¹⁴ (where the small spin-splitting terms are neglected):

$$E_n = E(n, B, k_z) \left[1 + \frac{K_2}{E_g} E(n, B, k_z) \right], \tag{4}$$

where $E(n, B, k_z) \equiv \omega_c^*(n + \frac{1}{2}) + k_z^2/2m^*$, $\omega_c^* = eB/m^*$ is the cyclotron energy, n is the LL index, and m^* is the electron band-edge mass in the QW material. The nonparabolicity parameter K_2 is given, from four-band $\mathbf{k} \cdot \mathbf{p}$ theory, by¹⁵

$$K_2 = - \frac{(1 - m^*)^2 E_g (3E_g + 4\Delta + 2\Delta^2/E_g)}{(E_g + \Delta)(3E_g + 2\Delta)}. \quad (5)$$

For GaAs, one obtains $K_2 = -0.83$, using in (5) the value $m^* = 0.067$ for the effective mass.¹⁶ It can be seen from Eq. (4) that nonparabolic effects are more important for high values of $E(n, B, k_z)$, as found in quantum wells due to the confinement energy.

In Ref. 3 magneto-optical data in GaAs QW's are fitted using (4) to describe the electron levels, with $m^* = 0.067$ but using the value $K_2 = -1.2$. This is an indication that the conduction-band nonparabolicity is enhanced with respect to the values predicted by simple models. We will come back to this point at the end of Sec. V.

IV. INTERBAND OPTICAL TRANSITIONS: MATRIX ELEMENTS AND SELECTION RULES

Let us consider the process in which a photon is absorbed and an electron is raised from a valence-band LL to a conduction-band one. We indicate with $|\Psi_n^I\rangle$ and $|\Psi_{n'}^F\rangle$, respectively, the initial (valence) and final (conduction) states with Landau index n, n' defined in (3a), whose envelope terms F_n^j depend implicitly on the magnetic field; the matrix element for direct optical transitions is given by

$$M_{n,n'} = \langle \Psi_n^I | \mathbf{p} \cdot \boldsymbol{\epsilon} | \Psi_{n'}^F \rangle = \sum_{i,j=1}^6 \langle u_i | \mathbf{p} \cdot \boldsymbol{\epsilon} | u_j \rangle \langle F_n^i | F_{n'}^j \rangle + \sum_{i,j=1}^6 \boldsymbol{\epsilon} \cdot \langle F_n^i | \mathbf{p} | F_{n'}^j \rangle \delta_{ij}, \quad (6)$$

$\boldsymbol{\epsilon}$ being a unit vector in the direction of the electric field of the incident radiation. We use here the compact notation

$$\begin{aligned} \langle u_i | (\dots) | u_j \rangle &\equiv \int_{\text{cell}} u_i^*(\mathbf{r}) (\dots) u_j(\mathbf{r}) d\mathbf{r}; \\ \langle F_n^i | (\dots) | F_{n'}^j \rangle &\equiv \int_{\text{crystal}} F_n^{i*}(\mathbf{r}) (\dots) F_{n'}^j(\mathbf{r}) d\mathbf{r}. \end{aligned} \quad (7)$$

The first term on the right-hand side of (6) gives the allowed interband transition matrix elements.¹⁷ The second term, which gives the strength of the intraband transitions analogous to those observed in cyclotron resonance and whose explicit expression is given in Appendix B, involves essentially the overlap between the same components of the wave function (2) for the two states I and F ; for this reason, it is expected to contribute also to the interband transition strengths in type-II superlattice systems like InAs/GaSb, where the conduction-band states of one material are strongly mixed with the valence-band states of the other, as a consequence of the peculiar band lineup of the InAs/GaSb heterojunction.⁷ In the present case we neglect this term since it gives a contribution to $|M_{n,n'}|^2$ which is typically 1–2% of that given by the first term.

The intensity of an inter-Landau level transition between the states I and F is thus proportional to the squared matrix element

$$\begin{aligned} |M_{n,n'}|^2 &= \left| \sum_{i,j=1}^6 \langle u_i | \mathbf{p} \cdot \boldsymbol{\epsilon} | u_j \rangle \int c_i^*(z) c_j(z) dz \right. \\ &\quad \left. \times \int \phi_{m_i}^* \phi_{m_j} d\mathbf{r} \right|^2 \\ &= \left| \sum_{i,j=1}^6 (\mathbf{p} \cdot \boldsymbol{\epsilon})_{ij} \int c_i^*(z) c_j(z) dz \delta_{m_i, m_j} \right|^2; \end{aligned} \quad (8)$$

m_i, m_j are the i th and j th components of the vectors $m = (n, n-1, n+1, n+1, n, n+2)$ and $m' = (n', n'-1, n'+1, n'+1, n', n'+2)$, respectively. Since the only matrix elements $(\mathbf{p} \cdot \boldsymbol{\epsilon})_{ij}$ different from zero, for circularly polarized light and in the Faraday configuration, are

$$\begin{aligned} |(\mathbf{p} \cdot \boldsymbol{\epsilon})_{12}| &= P/\sqrt{2} = |(\mathbf{p} \cdot \boldsymbol{\epsilon})_{46}| = \sqrt{3} |(\mathbf{p} \cdot \boldsymbol{\epsilon})_{13}|, \\ |(\mathbf{p} \cdot \boldsymbol{\epsilon})_{45}| &= |(\mathbf{p} \cdot \boldsymbol{\epsilon})_{13}| \end{aligned} \quad (9)$$

[P being the Kane momentum matrix element appearing in (1a)], one sees by inspection that the selection rule $n' - n = \pm 1$ must be satisfied, the plus (minus) sign referring to right- (left-) handed circular polarization (hereafter σ^+ and σ^-).

The matrix elements (8) for optical transitions in a magnetic field are proportional to the absorption coefficient. At zero field the evaluation of the absorption coefficient involves an integration over the in-plane momentum $k_{\parallel} \equiv (k_x, k_y)$, whereas in a magnetic field the Landau levels are degenerate and the integration over k_{\parallel} reduces to a factor which expresses such degeneracy.

We show in Table II how the various components of the wave function (2) are involved in the transitions for the two different polarizations σ^+ and σ^- , the arrows connecting the pairs of components which contribute to the overlap integral in (8): σ^+ corresponds to $\Delta m_J = +1$ and σ^- to $\Delta m_J = -1$, where m_J is the total angular momentum quantum number. A shorthand notation for the $|J; m_J\rangle$ basis states (3b) is introduced, as indicated in the left part of the table.

Note that the oscillator strength of an HH component is three times bigger than the LH one, as a consequence of the particular form of the atomiclike dipoles (9) associated with the basis set chosen (this is represented by the thicker lines in the table): transitions from HH Landau levels are thus expected to be more intense than those involving LH levels. Pairs connected by down-pointing arrows are expected to give a negligible contribution to (8) since the conduction (valence-) band components in a valence (conduction) state are always very small (1–3%). We stress the fact that in a simple scheme which uses only the selection rule $\Delta n = \pm 1$ for the total wave function to determine the allowed transitions between Landau levels, far more transitions are predicted than experimentally observed,⁴ because the mixing between LH and HH hole subbands, together with the restrictions imposed by Table II, make many of the allowed transitions have small matrix elements. Moreover, the mixing makes the transition intensities strongly field-dependent: the resulting picture of magneto-optical transitions is thus neither

TABLE II. Components of the Landau-level wave function [Eq. (2) in the text] involved in the optical transitions for the two different circular polarization.

		$ F_{n-1}\rangle$	$\xleftarrow{\sigma^-}$	$ F_n\rangle$	$\xrightarrow{\sigma^+}$	$ F_{n+1}\rangle$
CB \uparrow	$(s\uparrow\rangle)$	$n-1$	\leftarrow	n	\rightarrow	$n+1$
HH \uparrow	$(\frac{3}{2}, \frac{3}{2}\rangle)$	$n-2$	\leftarrow	$n-1$	\rightarrow	n
LH \uparrow	$(\frac{3}{2}, -\frac{1}{2}\rangle)$	n	\leftarrow	$n+1$	\rightarrow	$n+2$
CB \downarrow	$(s\downarrow\rangle)$	n	\leftarrow	$n+1$	\rightarrow	$n+2$
LH \downarrow	$(\frac{3}{2}, \frac{1}{2}\rangle)$	$n-1$	\leftarrow	n	\rightarrow	$n+1$
HH \downarrow	$(\frac{3}{2}, -\frac{3}{2}\rangle)$	$n+1$	\leftarrow	$n+2$	\rightarrow	$n+3$

simple nor obvious. In addition, even transitions that satisfy the restrictions of Table II can still have vanishing matrix elements due to the different parity of the envelope functions $c_j(z)$ of the initial and final state involved.

Thus the explicit evaluation of the dipole matrix elements (8) is an essential ingredient in any attempt to make a comparison between theory and experiment. Postponing this comparison to Sec. V, we discuss now briefly simple symmetry properties of the envelope functions $c_j(z)$ appearing in the overlap integrals in (8).

Every $c_j(z)$ in the envelope function (2) is a solution of a 1×1 effective Hamiltonian H_{eff} , obtained by projecting the Hamiltonian (1) onto the j th edge. It can be shown that H_{eff} , if flat-band conditions prevail, contains only even powers of $k_z \equiv -i\partial/\partial z$.¹⁸ Thus every $c_j(z)$ can be either even or odd with respect to the reflection $z \rightarrow -z$ in one of the mirror (x, y) planes bisecting the QW layer. In particular the HH \uparrow state is coupled, in the matrix (1a), with the LH \downarrow state by a term proportional to k_z , and to LH \uparrow by a term independent of k_z (see the left column of Table II for the notation). As k_z is odd under the reflection with respect to the mirror planes, an even HH \uparrow component will be coupled with an odd LH \downarrow and an even LH \uparrow , and vice versa. A similar argument applies to the coupling between HH \downarrow , LH \uparrow , and LH \downarrow states. To illustrate this point, we show in Fig. 2 the z dependence of the squared amplitudes $|c_j(z)|^2$ for each of the hole components ($j=2, 3, 5, 6$) of the envelope function (2) for the highest (in energy) four hole Landau levels with $n=1$ at $B=10$ T, in a 78-Å QW. The strong admixture between the HH and LH components is clearly visible in the LL2, LL3, and LL4 states: only the highest LL1 state displays a dominant HH \uparrow character. As anticipated, HH \uparrow (HH \downarrow) and LH \downarrow (LH \uparrow) states are mixed with opposite parity. The total wave function, not shown, does not exhibit any particular reflection symmetry.

It is worth noting that the mixing between LH and HH Landau levels at finite fields leads, as we shall see in the following, to the violation of the usual selection rule $\Delta m = \text{even integer}$, m and m' being the subband indices of the valence- (HH or LH) and conduction-band (CB) states involved in the transition. Even at $B=0$ transitions between subbands of different parity are equally allowed, due to valence-band hybridization at finite k_{\parallel} (Ref. 19) (such transitions, as the one between HH2 and

CB1 subbands, have also experimentally been observed²⁰). The correspondence between k_{\parallel} dispersion at $B=0$ and Landau-level behavior can be easily understood by noting that, in the limit of high oscillator quantum numbers, the Landau levels of a subband $E(k_y)$ are given by²

$$E_n(B) \simeq E(k_y = \sqrt{2eBn/c}), \quad n \gg 1.$$

In the following we will focus on the behavior of inter-band transitions at high magnetic fields which, for the range of energy of interest here, result from Landau levels of index $n \lesssim 10$. These states derive at $B \simeq 0$ from the region of subband structure around $k_{\parallel}=0$. Hence for these levels the limit $B \rightarrow 0$ is equivalent to the limit $k_{\parallel} \rightarrow 0$, where the HH and LH components are decoupled: This should be kept in mind especially when reading Sec. V. The full coupling provided by the off-diagonal elements in the Luttinger matrix Hamiltonian (1a) would be present at $B \sim 0$ in Landau levels with high

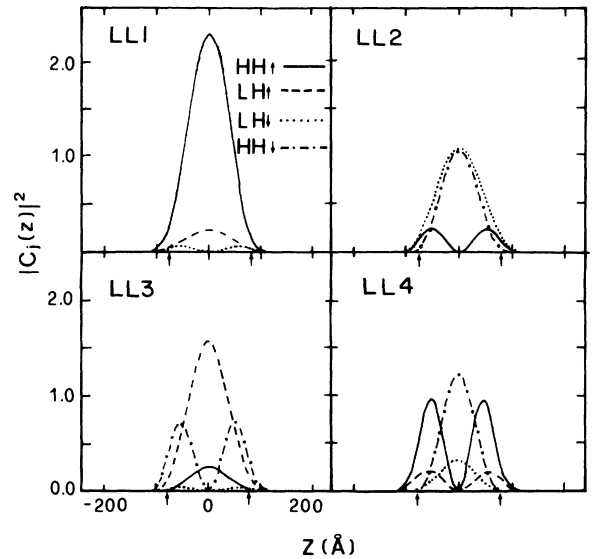


FIG. 2. Squared amplitudes associated with the four components (indicated in the first panel) of the envelope functions for the four highest valence states with Landau index $n=1$, at $B=10$ T. The levels are labeled with LL1, LL2, LL3, and LL4, in order of decreasing energy. The arrows show where the GaAs/ $\text{Al}_x\text{Ga}_{1-x}\text{As}$ interface is located.

oscillator index, i.e., those resulting from states of finite k_{\parallel} : In particular, valence-to-conduction-band transitions from high- n Landau levels originating from subbands of different parity would have finite dipole matrix elements at $B \simeq 0$ and the results of Ref. 19 would be recovered.

V. COMPARISON WITH THE EXPERIMENTS

We made a comparison with the results of excitation spectroscopy experiments performed in a nominally 80-Å GaAs quantum well²¹ clad between thick $\text{Al}_{0.3}\text{Ga}_{0.7}\text{As}$ layers, at high field (up to 20 T) and at very low temperature, in the Faraday configuration.⁵

An important input parameter in the calculation is the conduction-band discontinuity $Q_c = \Delta E_c / (E_g^{\text{AlGaAs}} - E_g^{\text{GaAs}})$: We have estimated this quantity by fitting the energy of the observed peaks at $B = 0$ as follows.²² The calculated dependence of the corresponding transition energies on Q_c is shown in Fig. 3, with solid lines. The arrows drawn on the left side indicate the experimental observed values, corrected for the binding energies of the excitons: We used for these latter quantities the theoretical values quoted in Ref. 23, obtained with a variational method (they range from ~ 6 meV for the binding energy of the HH1-CB1 exciton to ~ 10 meV for the LH1-CB1). We found that the best fit to experimental points is obtained assuming $Q_c \simeq 0.6$ (the bars drawn on the curves at this value account for a possible uncertainty of ± 2 Å on the GaAs well thickness): This esti-

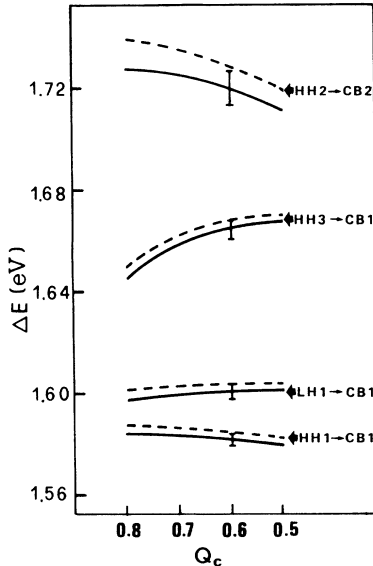


FIG. 3. Calculated dependence of the transition energies at $B = 0$ on the conduction-band discontinuity $Q_c \equiv \Delta E_c / \Delta E_g$. Solid lines are obtained with an electron mass $m^* = 0.074$, dashed lines with $m^* = 0.067$ (see text). The observed transitions, corrected for the binding energies of the excitons as explained in the text, are indicated by arrows. The bars drawn at $Q_c = 0.6$ account for a possible uncertainty of ± 2 Å in the well width.

mate is close to the recent and perhaps most accurate determinations of this parameter for the GaAs/ $\text{Al}_x\text{Ga}_{1-x}\text{As}$ system, $Q_c = 0.69 \pm 0.03$.²⁴

In Figs. 4(a) and 4(b) we show the calculated interband transition energies for both the polarizations of incident light, with intensities obtained from the transition matrix elements (8).²⁵ We adopt for convenience from now on the following convention to label transitions: the numbers indicate the Landau level indices n of the initial and final level, while the letters refer to the character of the subband at $B = 0$; the subscript m is the subband index. The two spin-split hole levels, for every Landau index n , will be identified (when necessary) by giving in parentheses the spin character at $B \simeq 0$, where the HH and LH mixing (for the low- n levels of interest here) is small.

We normalize intensities to the most intense transition, which turns out to be the -2 HH1(\downarrow) \rightarrow -1 CB1(\downarrow) in our notation (first line from below in the σ^+ spectrum), and plot only those which are at least 5% of that one. Solid lines represent transitions with a calculated intensity between 1.0 and 0.4; dashed lines represent those between 0.4 and 0.05. With dotted lines we indicate transitions which are smaller than 5% at some fields but acquire intensity through the admixture with other states with increasing magnetic field. In particular, this is true for transitions between low-index LL deriving from the HH2 and CB1 edges, which are parity forbidden at $B = 0$, but acquire intensity through the admixture with LH

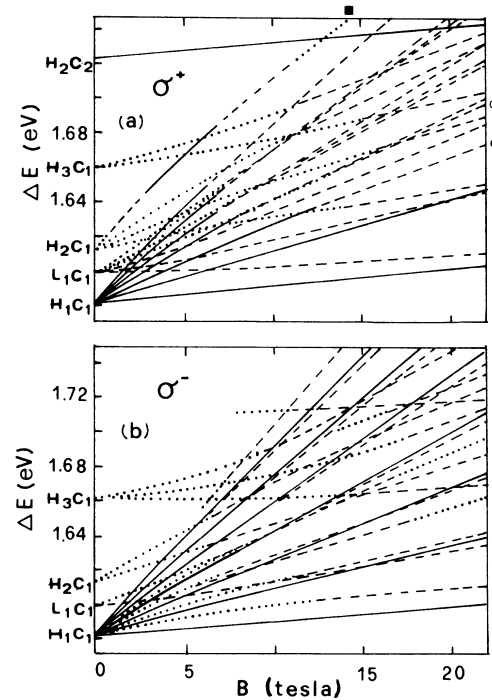


FIG. 4. Calculated transition energies for the two circular polarizations, as a function of the magnetic field B . Intensities are normalized to the lowest HH1-CB1 transition and are represented by dotted lines, intensity less than 0.05; dashed lines, between 0.05 and 0.4; solid lines, between 0.4 and 1. The HH1-CB1 transition is marked H_1C_1 , etc.

states with opposite parity at higher values of the magnetic field.

Many interesting features, that are not obvious on the basis of the calculated Landau levels only are emphasized by the present calculation. For instance, the admixture between LH and HH hole states in Landau levels with $n \geq 0$ leads, at fields above 10 T, to a change of slope of the transition lines involving these levels, making them less steep at higher fields where they recover in part the LH character (which, because of the particular asymmetry in the diagonal elements of the Luttinger hole Hamiltonian,¹³ has a heavier mass in the (k_x, k_y) plane).

One important consequence is that the zero-field exciton binding energy in QW's, obtained by extrapolation at $B=0$ of high-field data as the difference in energy between the ground state and the continuum states, may in some cases give an overestimated value for the binding energy: In fact the experimental values for this quantity, derived in the above manner,⁴ are systematically higher than the theoretical ones.^{26,27}

Note that, for the σ^- spectrum, the transitions associated with Landau levels that evolve from the zero-field HH1-CB1 edge are always stronger than those involving LH states. The more or less regular, equidistant Landau level-like features can in fact be recognized both in the experiment and the calculation. This statement is definitely not true in the more complicated σ^+ spectrum.

As an example of the effect of hole mixing on the transition strengths, we report in Fig. 5 the calculated intensities of the $0 \text{ HH1}(\downarrow) \rightarrow 1 \text{ CB1}(\downarrow)$ transition—curve (a)—and of the $0 \text{ LH1}(\downarrow) \rightarrow 1 \text{ CB1}(\downarrow)$ transition—curve (b)—as a function of the magnetic field B . [In Fig. 4(a) the corresponding transition lines are identified with a solid and empty circle, respectively.]

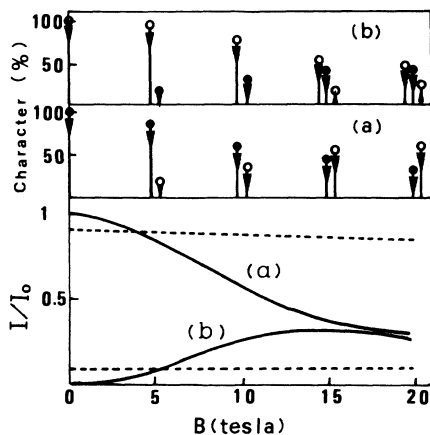


FIG. 5. Normalized intensities of the transition $0 \text{ HH1}(\downarrow) \rightarrow 1 \text{ CB1}(\downarrow)$ [curve (a)] and $0 \text{ LH1}(\downarrow) \rightarrow 1 \text{ CB1}(\downarrow)$ [curve (b)] as a function of the magnetic field B . In the upper part of the figure the weight of the various hole components in the envelope functions are shown for different values of B : solid and empty circles correspond respectively to heavy and light states while up- and down-pointing arrows identify the spin states. For comparison, the intensities of the corresponding transitions in *bulk* GaAs are shown with dashed lines.

On the top of each figure we show, as functions of B , the relative weights of the hole components entering into the envelope function of the Landau level. The $0 \text{ LH1}(\downarrow)$ and $0 \text{ HH1}(\downarrow)$ levels are both visible in Fig. 1(a), the $0 \text{ LH1}(\downarrow)$ being the one which crosses the B axis at about 13 T. Their anticrossing behavior is easily understood by recalling that the HH1 subband has a parallel mass [i.e., the mass in the (k_z, k_y) plane] lighter than the LH1 subband: The splitting of the possible crossing levels arises from the off-diagonal terms in (1a), with a resulting heavy mixing of the $m_J = \pm \frac{3}{2}$ and $m_J = \pm \frac{1}{2}$ character.

At zero field the transition (b) is forbidden, in σ^+ polarization, by the conservation of the total angular momentum, since for this transition $\Delta m_J = -1$, but at $B \neq 0$ it acquires intensity through the admixture of the hole level with a HH \downarrow component. At $B \gtrsim 15$ T the intensity decreases again due to an increase of a LH \uparrow component.

On the other hand, the transition (a), which is allowed at $B=0$, becomes less intense at higher fields due to the increasing mixing with the LH \downarrow component. For comparison, we report with dashed lines the intensities of the corresponding transitions in *bulk* GaAs: It is evident that mixing effects in QW systems make the transition intensities strongly field dependent.

A similar analysis (see Fig. 6) is performed on the $3 \text{ HH2}(\downarrow) \rightarrow 4 \text{ CB1}(\uparrow)$ transition, which is parity forbidden at $B=0$ [the corresponding line is identified with a square in Fig. 4(a)]: At $B \neq 0$ it grows in intensity as the mixing of the odd HH \downarrow state with a LH \uparrow component of the opposite parity makes a nonvanishing overlap with the even C state in the matrix element (8) (see Fig. 6). At fields higher than 8 T, a “forbidden” HH \uparrow component is picked up, making the intensity vanish again.

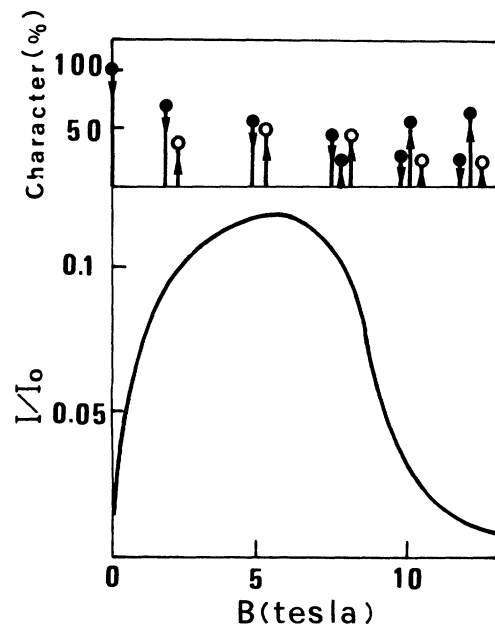


FIG. 6. Same as in Fig. 5, for the $3 \text{ HH2}(\downarrow) \rightarrow 4 \text{ CB1}(\uparrow)$ transition.

As it was already mentioned at the end of Sec. IV, for $B \rightarrow 0$ also transitions involving higher- n Landau levels should be considered. The above results are however meaningful and relevant at finite (and relatively large) values of B where the transitions in the range of energy of the experiments considered here come mainly from low-index Landau levels.

In Fig. 7, the calculated intensities versus magnetic field for the same two transitions of Fig. 5 are displayed, for three different values of the QW width. For the narrow well case the coupling between the two states starts to be effective at high fields, due to the marked difference in the confinement energies of the two holes: The intensities are thus slowly varying with the field and in particular the transition from the upper HH1 level (the one which is allowed at $B=0$) shows a closer resemblance to the corresponding bulk transition line (upper dashed line in figure). On the other hand, for the thick-well case, the mixing takes place at much lower fields, the upper level thus acquiring a dominant LH \downarrow character that makes the intensity decrease abruptly towards the corresponding bulk value (lower dashed line): In particular, this level becomes nearly flat after ~ 5 T, due to the anticrossing behavior with the lower Landau levels, displaying only a very weak dependence on the magnetic field. The partner transition from the lower LH1 level (thin line), after an initial increasing of strength due to the interchange of character between the two LL, is also depressed after ~ 5 T because of a strong mixing with a third "forbidden" LH \uparrow component.

We compare the outcome of our calculation with the experimental data by using band structure parameters that correctly reproduce the bulk data and proceed as follows.

We corrected our results for excitonic effects, in the same way as done in Ref. 3. The structure of the magneto-optical spectra in GaAs QW's has been interpreted by several authors^{4,5,28} in terms of transitions between free-carrier Landau levels, of which only the lowest is affected by excitonic effects. This is known, however, not to be

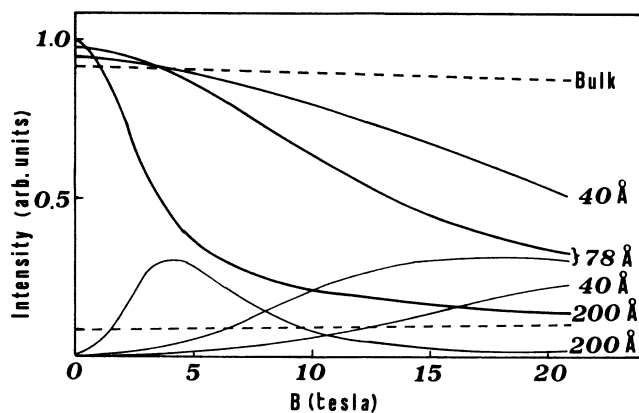


FIG. 7. Intensity vs magnetic fields plot for the same two transitions of Fig. 5, for three different values of the QW width (solid lines) and for the bulk (dashed lines).

the case in bulk GaAs in which Coulomb binding is appreciable at high fields even in the higher levels.²⁹ In a quantum well, due to the enhanced binding energy of excitons, the Coulomb interaction between electron and holes is expected to play a significant role in the interpretation of magneto-optical spectra.

In the theory of simple-band excitons in highly anisotropic systems in an external magnetic field described in Ref. 6, the high-field correction to the free Landau level energy due to Coulomb interaction is written as

$$E_B = 3R^*D_1 \left[\frac{eB}{2(2n'+1)\mu R^*} \right]^{1/2}, \quad n'=0,1,2,\dots \quad (10)$$

In (11) μ is the exciton reduced mass, R^* is an effective Rydberg $R^* = \mu e^4 / 2\epsilon^2$ (ϵ being the dielectric constant of the QW material) and D_1 is a parameter related to the dimensionality of the exciton ($D_1 = \frac{1}{4}$ in the 3D case, while $D_1 = 1$ for a strictly 2D exciton). Note that E_B does not depend on the reduced mass μ .

We subtracted the binding energy (10) from the calculated Landau level transition energies, taking $n'=0$ for the lowest line in each of the fans emerging from the zero-field edges in Figs. 4(a) and 4(b), $n'=1$ for the next, and so on. The best overall agreement with experimental points is obtained with $D_1 \simeq 0.5$. Formula (10) applies in the limit of high fields: A rough estimate of its domain of validity is given by the criterion $\gamma > 1$, where γ is the reduced magnetic field $\gamma = \omega_c^* / 2R^*$; taking $\mu^{-1} = 1/m^* + \gamma_1$,³⁰ one finds $B \geq 6$ T.

It must be remarked that the expression (10) is derived in the case of simple parabolic bands and thus should not be taken too seriously in the present context, whereas a realistic calculation of exciton binding energies in quantum wells should include at the beginning the coupling between heavy and light holes.

We then identify the transitions in Figs. 4(a) and 4(b) with the corresponding ones in the experimental results: this comparison shows that we could assign every experimental transition to a calculated one, but that consistently *all* theoretical ones were too steep, clearly indicating a too-small electron mass. We found that an increase of the electron effective mass at the band edge by $\sim 11\%$ is necessary to give the correct slopes of the transition lines.

The results of our calculation are reported in Figs. 8(a) and 8(b) (excitonic corrections included) together with the observed spectra, for $B > 6$ T. Although the transitions have the right slope, few of them have absolute energy slightly different from the observed ones (typically deviations of 2–5 meV are encountered). However the strongest lines, originating from the HH1-CB1 edge, come out at the right energy and with the right slope. We note that the effect of the exciton character of the transitions is essential in obtaining not only the right energy, but also the right slope for the transitions corresponding to the lowest three exciton states.

An additional downward shift of $\simeq 9$ meV has been imposed on the lowest HH1-CB1 and LH1-CB1 lines to fit approximately the HH1-CB1 exciton peaks. This value

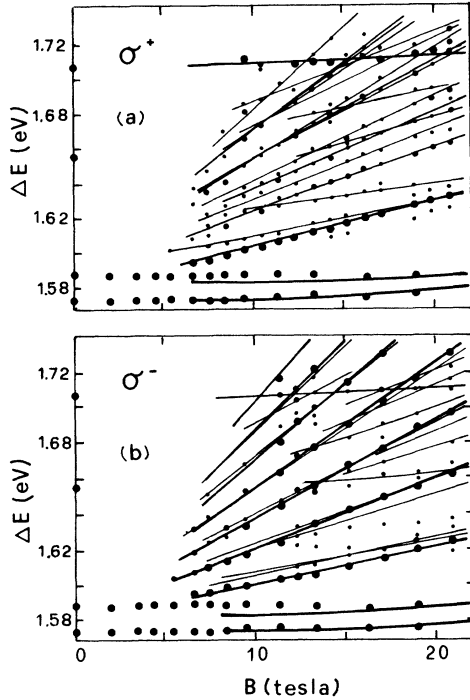


FIG. 8. Comparison between the calculated (lines) and the experimental transition energies (dots): Excitonic corrections are included, as explained in the text. Large dots correspond to strong transitions, small dots to the weak ones.

of the zero-field heavy-hole exciton binding energy agrees with the value of 9.4 meV derived from a photoluminescence study of an 80-Å GaAs/Al_{0.3}Ga_{0.7}As QW reported in Ref. 31. In Fig. 9 the predicted intensities at $B = 19$ T are compared with the experimental ones, for both polarizations: In order to mimic the broadening of the observed peaks, we have dressed each of the indicated intensity bars with a Lorentzian-shaped profile 7 meV wide (the two lowest exciton peaks are not shown in the figure). The differences between the observed σ^+ and σ^- spectra come out naturally from the calculation, making the overall agreement satisfactory. It should be remarked that a small change in the relative energy position of transition originating from different subbands, such as LH1-CB1 or HH2-CB1, has a sensitive effect on the observed spectra. Since the position of the subbands is extremely sensitive to the values of the material parameters (thickness, aluminum content, and mainly band-offset) an exact knowledge of the latter is required in order to make a successful comparison between theory and experiments.

A surprising fact is that we need to use a value for the electron mass at the edge of the conduction band [$m^* = 0.074$, corresponding to the value $P = 8.85$ eV Å in (1a)] higher than the commonly adopted value $m^* = 0.067$.¹⁶ We have also tried to analyze samples used in different experiments^{3,32} and consistently arrived at the same conclusion, i.e., a *higher* electron mass is needed to fit the experimental data.

At present is not possible to state unambiguously whether this effect is due to the quantum well, or to a

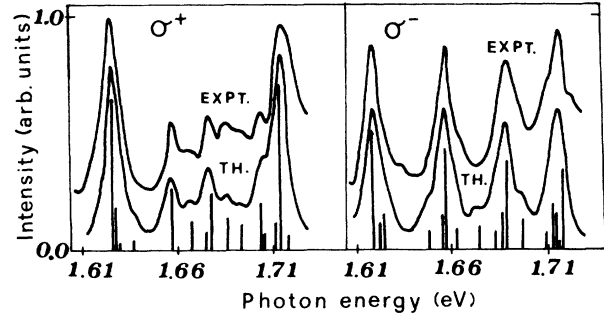


FIG. 9. Comparison between the excitation spectra measured at $B = 19$ T and the predicted intensities, for the two circular polarizations σ^+ and σ^- of the incident light. The theoretical curves have been obtained by dressing each of the calculated intensity bars with Lorentzian-shaped profiles 7 meV wide.

higher nonparabolicity of the bulk or to the approximate treatment of the exciton: we have verified however that the *bulk* GaAs magnetoabsorption spectra³⁹ are reproduced in detail by a calculation of inter-Landau-level transitions when the value $m^* = 0.067$ is used. Both the effect of the exciton and that of enhanced nonparabolicity is to reduce the slope of the transition energies as a function of the field B ; therefore the two effects cannot easily be distinguished. The position of the subbands at zero magnetic field is only weakly dependent on the mass used in the range of uncertainty relevant here (for comparison we show in Fig. 3 this dependence). There are several indications that the bulk GaAs nonparabolicity is indeed stronger than that predicted by the six-band model used here:^{33,34} However, a clear distinction between the two effects requires a careful treatment of the effect of the exciton, the complex valence-band structure, and the magnetic field effect simultaneously.

VI. CONCLUSIONS

In conclusion, the results of interband magneto-optical measurements of GaAs quantum wells are compared with the calculated transition energies. The explicit evaluation of the transition matrix elements is necessary in order to understand qualitatively all the essential features of the observed spectra, and demonstrate the important effect of hole subband mixing: These effects are shown to be more pronounced in quantum wells than in bulk materials. Furthermore, the inclusion of excitonic corrections in a simplified manner leads to a detailed agreement between experimental and theoretically calculated spectra. However, a quantitative agreement is reached only if an electron mass higher than the commonly accepted value is assumed: we attribute this discrepancy either to the effect of higher GaAs nonparabolicity and/or to the effect of excitons.

Note added. A paper has been published³⁵ in which a theory of excitons in a magnetic field normal to the quantum well is constructed, including the complex valence-band structure. All the observable optical transitions are found to involve bound excitons and the exciton lines are significantly different in energy from the unbound

electron-hole pair lines; moreover, due to the LH and HH mixing at finite fields, excitonic states cannot be attributed a purely light or heavy hole character. This effect is brought about mainly by the magnetic field which mixes the hole levels. This mixing is correctly accounted for by our calculation even if our treatment of the Coulomb interaction is more approximate. One striking point of disagreement with our results is that, in σ^- polarization, the second transition line of lowest energy is attributed to the $3d$ HH exciton, rather than to the $1s$ LH exciton.

ACKNOWLEDGMENTS

This work is part of the Scuola Internazionale di Studi Superiori Avanzati (SISSA)–CINECA computer center joint project, sponsored by the Italian Ministry of Education. Two of the authors, F.A. and A.F., also acknowledge partial financial support by Gruppo Nazionale Struttura della Materia–Centro Interuniversita di Struttura della Materia.

APPENDIX A

We show in the following how the anomalous low-field dispersion of the LH1 subband in Fig. 1(a) can be understood simply in terms of the interaction between LH1 and the second HH2 subband.

The bulk valence-band top is well described by the 4×4 Luttinger Hamiltonian that can be obtained by removing rows and columns 1 and 4 in (1a), corresponding to the conduction-band states: the coupling with these states is taken into account by using the renormalized band parameters γ_1^L , γ_2^L , γ_3^L , and κ^L ; ³⁶ the envelope functions are given by an expression similar to (2) but with the first and fourth components missing. Let us consider for simplicity the case $n = -1$. Thus, as it is apparent from (2), only HH \downarrow and LH \uparrow states enter into the

wave function (see the left side of Table II, the labeling of states). If we let the a, a^\dagger operators appearing in the Luttinger Hamiltonian act on the harmonic oscillator functions ϕ_n of (2), the following 2×2 matrix is obtained:

$$H = \begin{pmatrix} A & R \\ R & D \end{pmatrix}, \quad (\text{A1})$$

where

$$\begin{aligned} A &= -(\gamma_1^L + 2\gamma_2^L) \frac{k_z^2}{2} - \frac{eB}{2c} (\gamma_1^L - \gamma_2^L - \kappa^L), \\ D &= -(\gamma_1^L - 2\gamma_2^L) \frac{k_z^2}{2} - \frac{3eB}{2c} (\gamma_1^L + \gamma_2^L - \kappa^L), \\ R &= -\gamma_3 \sqrt{6eB/c} k_z, \end{aligned}$$

and k_z is the wave-vector component parallel to the QW axis.

In the absence of the linear k_z coupling, the A and D terms would give the dispersion relation of a purely light and heavy hole, respectively, characterized by effective masses in the z direction $m_{\text{HH,LH}}^* = (\gamma_1^L \mp 2\gamma_2^L)^{-1}$: let $C_{\text{LH},m}(z), C_{\text{HH},m'}(z)$ represent the corresponding eigenfunctions, when the QW boundary conditions are taken into account (m and m' thus being discrete quantum numbers). In (A1) k_z has to be replaced by $-i\partial/\partial z$, according to the usual prescription of the effective-mass theories; ³⁷ we seek for a solution F of the associated EM equations $\sum_{i,j} H_{ij} F_j = E F_i$ of the form

$$F = \begin{pmatrix} \alpha C_{\text{LH},m}(z) \\ \beta C_{\text{HH},m'}(z) \end{pmatrix}. \quad (\text{A2})$$

The EM equations can be recasted in the form of a system of two algebraic equations in the unknown coefficients α and β : solutions of the system exist if

$$\det \begin{pmatrix} \langle C_{\text{LH},m} | A - E | C_{\text{LH},m} \rangle & \langle C_{\text{LH},m} | R | C_{\text{HH},m'} \rangle \\ \langle C_{\text{LH},m} | R | C_{\text{HH},m'} \rangle^* & \langle C_{\text{HH},m'} | D - E | C_{\text{HH},m'} \rangle \end{pmatrix} = 0. \quad (\text{A3})$$

In a symmetric QW potential $C_{\text{LH}}, C_{\text{HH}}$ are either even or odd with respect to the reflection $z \rightarrow -z$; since $R \propto -i\partial/\partial z$, the off-diagonal matrix elements in (A3) are different from zero only if the two states have different parity: thus the first ($m = 1$) LH1 state will interact essentially with the second ($m' = 2$) HH2 state.

Let $E_\pm(B)$ represent the two roots of Eq. (A3) for this choice of the C_{LH} and C_{HH} states, the upper sign referring to the solution with highest energy. The inverse effective masses in the (k_x, k_y) plane, for the two levels, are proportional to

$$\left. \frac{dE_\pm}{dB} \right|_{B=0} = -\frac{e}{2c} \left[2\gamma_1^L + \gamma_2^L - 2\kappa^L + \text{sgn}(E_{0,\text{LH1}} - E_{0,\text{HH2}}) (\gamma_1^L + 2\gamma_2^L - \kappa^L) \mp \frac{12 | \langle k_z \rangle |^2 \gamma_3^{L^2}}{|E_{0,\text{LH1}} - E_{0,\text{HH2}}|} \right] \quad (\text{A4})$$

where $E_{0,\text{LH1}}, E_{0,\text{HH2}}$ are the zero-field confinement energies of the two holes:

$$\begin{aligned} E_{0,\text{LH1}} &= \frac{1}{2} (\gamma_1^L + 2\gamma_2^L) \left\langle C_{\text{LH},1} \left| \frac{\partial^2}{\partial z^2} \right| C_{\text{LH},1} \right\rangle, \\ E_{0,\text{HH2}} &= \frac{1}{2} (\gamma_1^L - 2\gamma_2^L) \left\langle C_{\text{HH},2} \left| \frac{\partial^2}{\partial z^2} \right| C_{\text{HH},2} \right\rangle, \end{aligned} \quad (\text{A5})$$

and $\langle k_z \rangle$ is defined as

$$\langle k_z \rangle \equiv \left\langle C_{\text{LH},1} \left| -i \frac{\partial}{\partial z} \right| C_{\text{HH},2} \right\rangle. \quad (\text{A6})$$

Let us consider the simplest case of an infinite square-well potential of width L ; then $C_{\text{LH},1} = \sqrt{2/L} \sin(\pi z/L)$, $C_{\text{HH},2} = \sqrt{2/L} \sin(2\pi z/L)$, and

$$\begin{aligned}
E_0(\text{LH1}) &= -\frac{1}{2}(\gamma_1^L + 2\gamma_2^L)(\pi/L)^2, \\
E_0(\text{HH2}) &= -\frac{1}{2}(\gamma_1^L - 2\gamma_2^L)(2\pi/L)^2, \\
\langle k_z \rangle &= 8i/3L.
\end{aligned}
\tag{A7}$$

Substituting (A7) in (A4) and using the material parameters appropriate for GaAs (Ref. 38) $\gamma_1^L=6.85$, $\gamma_2^L=2.1$, $\gamma_3^L=2.9$, $\kappa^L=1.2$, it turns out that $(dE_-/dB)_0 > 0$, i.e., the upper $n = -1$ level has an initial electronlike dispersion.

It must be noted that this state is the HH2 in the infinite square well, whereas the finite barriers have the effect to push the LH1 edge above it [see Fig. 1(a)].

APPENDIX B

The second term in (6) can be rewritten in the following form:

$$M_{n,n'}^{(2)} = \sum_i \langle F_n^i | \mathbf{p} \cdot \boldsymbol{\epsilon} | F_{n'}^i \rangle \simeq m_0 \sum_{ij} \langle F_n^i | (\hat{\mathbf{v}} \cdot \boldsymbol{\epsilon})_{ij} | F_{n'}^j \rangle
\tag{B1}$$

[see (7) for the notation]. Here, instead of the first-principles scalar interaction $\mathbf{p} \cdot \boldsymbol{\epsilon}$, the matrix interaction term $m_0 \hat{\mathbf{v}} \cdot \boldsymbol{\epsilon}$ has been used;³⁹ the velocity operator $\hat{\mathbf{v}}$ is defined in terms of the Hamiltonian (1a) as

$$(\hat{v}_\alpha)_{ij} \equiv \frac{\partial (H_{\text{ax}})_{ij}}{\partial k_\alpha}
\tag{B2}$$

and is also a 6×6 matrix acting on the envelope functions

F_n defined in (2). For circularly polarized light, $\epsilon_z = 0$; then $\boldsymbol{\epsilon} \cdot \mathbf{v} = \epsilon_+ v_- + \epsilon_- v_+$, where $\epsilon_\pm \equiv (\epsilon_x \pm i\epsilon_y)/\sqrt{2}$ and

$$\begin{aligned}
v_\pm &= (v_x \pm iv_y)/\sqrt{2} = \frac{1}{\sqrt{2}} \left[\frac{\partial H_{\text{ax}}}{\partial k_x} \pm i \frac{\partial H_{\text{ax}}}{\partial k_y} \right] \\
&= (c/eB)^{1/2} \frac{\partial H_{\text{ax}}}{\partial a^\mp} = \mp (c/eB)^{1/2} [a^\pm, H_{\text{ax}}].
\end{aligned}
\tag{B3}$$

In (B3) we define the creation (a^+) and annihilation (a^-) operators¹⁷ as $a^\pm = (c/2eB)^{1/2} (k_x \pm ik_y)$, respectively.

$$M_{n,n'}^{(2)} = (c/eB)^{1/2} (E_F - E_I) \epsilon_\pm \sum_i \langle F_n^i | a^\mp | F_{n'}^i \rangle,
\tag{B4}$$

E_I, E_F being the energies of the initial and final levels. From the definition (2) and from the orthogonality of the oscillator states with different index n , one derives immediately the selection rule $\Delta n = \pm 1$, where the $+$ ($-$) sign holds for left (right) circularly polarized light. We underline the fact that the above selection rule pertains to the axial model only: If one uses the exact Hamiltonian (1), including the cubic part (1b) and the terms that come in when the crystal lacks inversion symmetry,⁹ the previous selection rule must be relaxed and one has instead $\Delta n = \pm m$, m an odd integer.⁴⁰ The matrix element (B4) has been used in this form in connection with the interpretation of cyclotron-resonance experiments in 2D hole gas in GaAs/Al_xGa_{1-x}As heterostructures.¹²

- ¹S. S. Nedorezov, *Fiz. Tverd. Tela (Leningrad)* **12**, 2269 (1970) [*Sov. Phys.—Solid State* **12**, 1814 (1972)].
²A. Fasolino and M. Altarelli, *Two-Dimensional Systems, Heterostructures and Superlattices*, edited by G. Bauer, F. Kuchar, and H. Heinrich (Springer, Berlin, 1984).
³D. C. Rogers, J. Singleton, R. J. Nicholas, C. T. Foxon, and K. Woodbridge, *Phys. Rev. B* **34**, 4002 (1986).
⁴J. C. Maan, A. Fasolino, G. Belle, M. Altarelli, and K. Ploog, *Phys. Rev. B* **30**, 2253 (1984).
⁵J. C. Maan, A. Fasolino, G. Belle, M. Altarelli, and K. Ploog, in *Proceedings of the 17th International Conference on the Physics of Semiconductors*, edited by J. D. Chadi and W. A. Harrison (Springer, New York, 1985).
⁶O. Akimoto and H. Hasegawa, *J. Phys. Soc. Jpn.* **22**, 181 (1967).
⁷M. Altarelli, *Phys. Rev. B* **28**, 842 (1983), and in *Applications of High Magnetic Fields in Semiconductor Physics*, edited by G. Landwehr (Springer, Berlin, 1983).
⁸M. Altarelli and A. Fasolino, *Highlights of Condensed Matter Theory*, edited by F. Bassani, F. Fumi, and M. P. Tosi (North-Holland, Amsterdam, 1985).
⁹E. O. Kane, *Semiconductors and Semimetals*, edited by K. Wilkerson and A. C. Beer (Academic, New York, 1966).
¹⁰L. M. Roth, B. Lax, and S. Zwerdling, *Phys. Rev.* **114**, 90 (1959).
¹¹S. R. Yang, D. Broido, and L. J. Sham, *Phys. Rev. B* **32**, 6630 (1985).
¹²E. Bangert and G. Landwehr, *Surf. Sci.* **170**, 593 (1986).

- ¹³J. M. Luttinger, *Phys. Rev.* **102**, 1030 (1956).
¹⁴E. D. Palik, G. S. Picus, S. Teitler, and R. F. Wallis, *Phys. Rev.* **122**, 475 (1971).
¹⁵G. Lindemann, R. Lassnig, W. Seidenbush, and E. Gornik, *Phys. Rev. B* **28**, 4693 (1983).
¹⁶J. M. Chamberlain, P. E. Simmonds, R. A. Stradling, and C. C. Bradley, in *Proceedings of the 11th International Conference on the Physics of Semiconductors, Warsaw, 1972* (PWN—Polish Scientific, Warsaw, 1972).
¹⁷C. R. Pidgeon and R. N. Brown, *Phys. Rev.* **146**, 575 (1966).
¹⁸P. Voisin, G. Bastard, and M. Voos, *Phys. Rev. B* **29**, 835 (1984).
¹⁹G. D. Sanders and Y. C. Chang, *Phys. Rev. B* **32**, 5517 (1985).
²⁰R. C. Miller, A. C. Gossard, G. D. Sanders, Y. C. Chang, and J. N. Schulman, *Phys. Rev. B* **32**, 8452 (1985).
²¹Subsequent informations have revealed that the 90-Å sample of Ref. 5 had in fact an 80-Å well thickness.
²²M. H. Meynadier, C. Delalande, G. Bastard, and M. Voos, *Phys. Rev. B* **31**, 5539 (1985).
²³J. A. Brum and G. Bastard, *J. Phys. C* **18**, L789 (1985).
²⁴J. Menendez, A. Pinczuk, D. J. Werder, A. C. Gossard, and J. H. English, *Phys. Rev. B* **33**, 8863 (1986).
²⁵F. Ancilotto, A. Fasolino, and J. C. Maan, *Superlatt. Microstruct.* **3**, 187 (1987).
²⁶R. C. Miller, D. A. Kleinmann, W. T. Tsang, and A. C. Gossard, *Phys. Rev. B* **24**, 1134 (1981).
²⁷R. L. Green, K. K. Bajaj, and D. E. Phelps, *Phys. Rev. B* **29**, 1807 (1984).

- ²⁸S. Tarucha, H. Okamoto, Y. Iwasa, and N. Miura, *Solid State Commun.* **52**, 815 (1984).
- ²⁹Q. H. F. Vreken, *J. Phys. Chem. Solids* **29**, 129 (1968).
- ³⁰M. Altarelli, *Band Structure, Impurities and Excitons in Superlattices*, Lecture Notes for the Winter School on Semiconductor Heterojunctions and Superlattices, Les Houches, 1985 (unpublished).
- ³¹A. Petrou, G. Waytena, X. Liu, J. Ralston, and G. Wicks *Phys. Rev. B* **34**, 7436 (1986).
- ³²B. Deveaud, A. Regreny, A. Romestein, and J. C. Maan (private communication).
- ³³U. Rossler, *Solid State Commun.* **49**, 943 (1984).
- ³⁴M. Braun and U. Rossler, *J. Phys. C* **18**, 3365 (1985).
- ³⁵S. R. E. Yang and L. J. Sham, *Phys. Rev. Lett.* **58**, 2598 (1987).
- ³⁶M. F. N. Schuurmans and G. W. t'Hooft, *Phys. Rev. B* **31**, 8041 (1985).
- ³⁷J. M. Luttinger and W. Kohn, *Phys. Rev.* **97**, 869 (1955).
- ³⁸K. Hess, D. Bimberg, N. O. Lipari, J. U. Fischbach, and M. Altarelli, *Proceedings of the 13th International Conference on the Physics of Semiconductors, Rome, 1976*, edited by F. G. Fumi (North-Holland, Amsterdam, 1976).
- ³⁹R. Grisar, H. Wachernig, G. Bauer, J. Wlasak, J. Kowalski, and W. Zawadzky, *Phys. Rev. B* **18**, 4355 (1978).
- ⁴⁰H. R. Trebin, U. Rossler, and R. Ranvaud, *Phys. Rev. B* **20**, 686 (1979).
- ⁴¹H. J. Lee, Y. Yuravel, J. C. Woolley, and A. J. Springthorpe, *Phys. Rev. B* **21**, 658 (1980).